

# Three-dimensional modeling of mass transfer in close binary systems with non-synchronous rotation

Bisikalo D.V.<sup>1</sup>, Boyarchuk A.A.<sup>1</sup>,  
Kuznetsov O.A.<sup>2</sup>, Chechetkin V.M.<sup>2</sup>

<sup>1</sup> *Institute of Astronomy of the Russian Acad. of Sci., Moscow*  
bisikalo@inasan.rssi.ru; aboyar@inasan.rssi.ru

<sup>2</sup> *Keldysh Institute of Applied Mathematics, Moscow*  
kuznecov@spp.keldysh.ru; chech@int.keldysh.ru

**Abstract**—We present the results of three-dimensional numerical simulations of mass transfer in semi-detached binary systems in which the mass-losing star is rotating. The cases of aligned and misaligned non-synchronous rotation of the donor star are considered; the resulting flow patterns are compared to the synchronous case. The main properties of the flow, such as the formation of an circumbinary envelope, the absence of a "hot spot" on the edge of the accretion disk, and the formation of a shock wave along the flow edge, are qualitatively similar to those obtained earlier. For the case of misaligned, non-synchronous rotation, the behavior of the disk and surrounding matter in established flow regime reflects changes in the boundary conditions at the surface of the donor star; in other words, a "driven disk" model is realized in the calculations.

## INTRODUCTION

Since the discovery of non-synchronous rotation (when the rotational velocity of one or both components differs from the orbital angular velocity of the system) by Schlesinger in the spectral binary  $\delta$  Lib in 1909 and in the eclipsing binary  $\lambda$  Tau in 1910 [1], non-synchronous rotation has been detected in numerous binary systems of various types. For a number of Algol-type systems (RZ Sct, U Cep, RY Per), there is evidence for the rapid rotation of one of the components [2, 3]. According to [2, 3], the degree to which the rotation is non-synchronous  $f = \Omega_*/\Omega$

is rather high for these systems:  $f = 6.6 \div 9.0$  for RZ Sct and  $f = 10.8 \div 14.5$  for RY Per. The presence of rotation for one component that differs from the orbital rotational velocity has also been detected for several long-period RS CVn stars (TZ For,  $\lambda$  And, AY Cet [4] and  $\alpha$  Aur (Capella) [5, 6]). The estimated rotation non-synchronicity of the hot star in the  $\alpha$  Aur system reaches  $f \sim 10 \div 12$  [7–9].

For a number of binary systems, various observational properties (light curves, radial velocity curves, etc) also appear to show long-period variations on timescales substantially longer than the orbital period. Among the best known binaries of this type are the systems Her X-1 (HZ Her) and SS433. In order to explain the long-period variations in the Her X-1 system, a "driven disk" model was suggested in [10–12], based on the idea that the rotation of the donor star is non-synchronous and misaligned. A similar model was also considered later for SS433 [13–17].

The first attempts to study the role of non-synchronicity in mass transfer were made in a ballistic approximation [9, 18]. However, the fact that gas-dynamical factors were not taken into account in these calculations casts doubt on the reliability of the results. Due to the three-dimensional nature of the problem, a correct analysis of the flow pattern in systems with non-synchronous rotation is possible only in the framework of 3D gas-dynamical models. Model calculations for binary systems with non-synchronously rotating components were presented in [19, 20]. Unfortunately, these studies used a simplified formulation of the problem, and did not take into account the change of the shape of the donor star in the case of non-synchronous rotation [21]; therefore, the results obtained require additional verification. In addition, the solution given in [19, 20] was limited, since the impact of the circumbinary gas on the flow structure near the donor star was not taken into consideration. Calculations made later [22–25] for the case of synchronous rotation indicated that the influence of the circumbinary gas can substantially change the structure of gaseous flows in the vicinity of  $L_1$  in a steady-state flow regime. Here, we present results for our solutions to this problem formulated in a self-consistent way, devoid of the drawbacks of previous models.

## 1 THE MODEL

### 1.1 Binary system parameters

In our previous studies [22, 23], we considered the flow morphology in a low-mass X-ray binary system with synchronously rotating components in a three-dimensional formulation. In order to study the impact of non-synchronous rotation of the donor star on the flow structure, we now consider a semi-detached system with the same parameters as those in [22, 23]. We adopted typical parameters for a low-mass X-ray binary, close to these of X1822–371 [26]. The primary

component was assumed to fill its Roche lobe and to have a mass  $M_1 = 0.28M_\odot$  and surface temperature  $T = 10^4$  K; the mass  $M_2$  of the secondary, a compact object with radius  $0.05R_\odot$ , was assumed to be  $1.4M_\odot$ . The orbital period of the system was  $P_{orb} = 5^h.56$ , and the distance between the centers of the components was  $A = 1.97R_\odot$ .

We will use the following terminology. We will call "synchronous" the case when all periods—i.e., the rotation periods of both of the stars and of the system as a whole—coincide ( $P_{\star 1} = P_{\star 2} = P_{orb}$ ); "non-synchronous" rotation is the case when the rotation period of the donor star does not coincide with the orbital rotation period. For non-synchronous rotation of the donor star, two positions of its rotation axis relative to the system are possible: 1) aligned, when the rotation axis of the donor star is perpendicular to the orbital plane of the binary system; and 2) misaligned, when this axis is inclined to this direction. For all calculations, we will assume that the rotation axis of the donor star goes through its center of mass and is fixed in the laboratory frame.

We assumed that the rotation velocity of the donor star in the laboratory frame is twice the orbital rotation velocity of the system. Three-dimensional calculations were performed for both aligned and misaligned rotation of the donor star.

## 1.2 Shape of the mass-losing star

The shape of the mass-losing component in a semi-detached binary system can easily be determined for the standard case, when it is assumed that: (i) the orbits of the components are circular, (ii) the rotation of the star is synchronized with the orbital rotation  $\Omega_\star = \Omega$ , and (iii) the stars are strongly concentrated, so that their gravitational fields can be considered to be the fields of point masses. Under these conditions, in the adopted coordinate frame (the  $X$  axis is directed along the line connected the centers of the stars, the  $Z$  axis coincides with the rotation axis, and the  $Y$  axis forms a right-handed coordinate system whose origin is at the center of mass of the donor star), the total potential in the Roche approximation can be written

$$\Phi(\mathbf{r}) = -\frac{GM_1}{d_1} - \frac{GM_2}{d_2} - \frac{1}{2}\Omega^2 \left( (x - x_c)^2 + y^2 \right) \quad (1)$$

and the shape of the donor star coincides with its Roche lobe; i.e., with the equipotential surface passing through the inner Lagrange point  $L_1$  (see, for example, [27, 28]). When the star reaches the boundary of its Roche lobe, mass transfer begins through  $L_1$ , where the pressure gradient is not balanced by other forces. In (1),  $M_1$  and  $M_2$  are the masses of the components,  $M = M_1 + M_2$  is the total mass of the system,  $\Omega$  is the orbital angular velocity of the system,  $\Omega = (0, 0, \Omega)$ ;  $x_c = AM_2/M$ ;  $d_1 = \sqrt{x^2 + y^2 + z^2}$  is the distance to the center of

mass of the primary (the donor star),  $d_2 = \sqrt{(x - A)^2 + y^2 + z^2}$  is the distance to the center of mass of the accretor, and  $A$  is the distance between the components.

The situation changes when the Roche approximation is not satisfied, so that the potential has a shape that differs from (1). Let us consider the general case, when the mass-losing component rotates non-synchronously and its rotation is misaligned with the orbital rotation:  $\boldsymbol{\Omega}_\star \not\parallel \boldsymbol{\Omega}$ . Following [29, 30], where the potential for the case of non-synchronous rotation is considered, and [21, 31, 32], where misaligned rotation is taken into account, we will determine the position of the Lagrange points, where the pressure gradient is not compensated by other forces. Assuming that  $\boldsymbol{\Omega}_\star$  does not change with time (there is no precession) and that the rotation of the star is uniform [21, 33], we can write the equation of motion for a test particle in a reference frame rotating with angular velocity  $\boldsymbol{\Omega}_\star$  in the form (without account for the pressure force):

$$\ddot{\mathbf{r}} = -\text{grad} \left( -\frac{GM_1}{d_1} - \frac{GM_2}{d_2} \right) - \ddot{\mathbf{r}}_0 - \boldsymbol{\Omega}_\star \times [\boldsymbol{\Omega}_\star \times \mathbf{r}] - 2\boldsymbol{\Omega}_\star \times \dot{\mathbf{r}},$$

where  $\ddot{\mathbf{r}}_0$  denotes the acceleration of the coordinate origin (the donor star's center of gravity) in the laboratory frame:

$$\ddot{\mathbf{r}}_0 = \boldsymbol{\Omega} \times [\boldsymbol{\Omega} \times (-\mathbf{r}_c)] = (\Omega^2 x_c, 0, 0)$$

$$\mathbf{r}_c = (x_c, 0, 0).$$

We obtain after simple manipulation

$$\ddot{\mathbf{r}} = \mathbf{F}$$

$$\mathbf{F} = -\text{grad} \left( -\frac{GM_1}{d_1} - \frac{GM_2}{d_2} \right) - \boldsymbol{\Omega} \times [\boldsymbol{\Omega} \times (-\mathbf{r}_c)] - \boldsymbol{\Omega}_\star \times [\boldsymbol{\Omega}_\star \times \mathbf{r}] - 2\boldsymbol{\Omega}_\star \times \dot{\mathbf{r}}.$$

The positions of the Lagrange points can be determined from the condition  $\mathbf{F} = 0$ . When there exists a potential  $\Psi$  such that  $\mathbf{F} = -\text{grad} \Psi$ , these points are stationary points of the potential. Using the relations

$$-\boldsymbol{\Omega} \times [\boldsymbol{\Omega} \times (-\mathbf{r}_c)] = (-\Omega^2 x_c, 0, 0) = -\text{grad} (\Omega^2 x_c x)$$

$$-\boldsymbol{\Omega}_\star \times [\boldsymbol{\Omega}_\star \times \mathbf{r}] = -\text{grad} \left( -\frac{1}{2} \Omega_\star^2 \Delta^2 \right),$$

where  $\Delta$  is the distance from the point  $\mathbf{r}$  to the rotation axis  $\boldsymbol{\Omega}_\star$ , we find that the desired potential  $\Psi$  has the form

$$\Psi(\mathbf{r}) = -\frac{GM_1}{d_1} - \frac{GM_2}{d_2} + \Omega^2 x_c x - \frac{1}{2} \Omega_\star^2 \Delta^2, \quad (2)$$

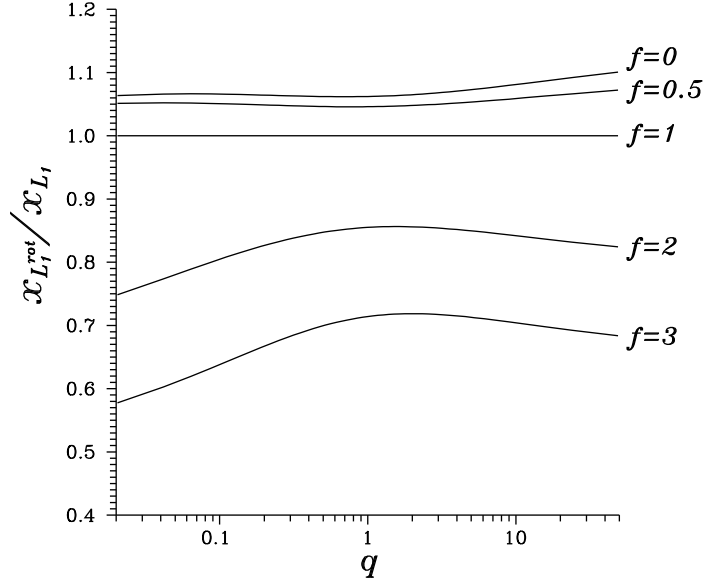


Figure 1: *Relative change of the position of the inner Lagrange point for systems with non-synchronous rotation  $x_{L_1^{rot}}/x_{L_1}$  as a function of the mass ratio of the components  $q = M_2/M_1$  for various values of the degree of non-synchronicity of the rotation  $f = \Omega_\star/\Omega$ .*

and the equation of motion can now be represented

$$\ddot{\mathbf{r}} = -\text{grad } \Psi - 2\boldsymbol{\Omega}_\star \times \dot{\mathbf{r}}.$$

The potential  $\Psi$  includes all forces acting in the rotating reference frame, except for the Coriolis force and the pressure gradient. For the special case of aligned rotation ( $\boldsymbol{\Omega}_{\star x} = \boldsymbol{\Omega}_{\star y} = 0$ )  $\Delta^2 = x^2 + y^2$  and the potential (to within a constant) is described by the expression

$$\Psi(\mathbf{r}) = -\frac{GM_1}{d_1} - \frac{GM_2}{d_2} - \frac{1}{2}\Omega^2 \left( (x - x_c)^2 + y^2 \right) - \frac{1}{2}(\Omega_\star^2 - \Omega^2) (x^2 + y^2). \quad (3)$$

Note that, in the case of aligned, synchronous rotation ( $\boldsymbol{\Omega}_\star = \boldsymbol{\Omega}$ ), the potential coincides with (1).

Using relations (1) and (3), we can determine the change of the position of the inner Lagrange point  $L_1^{rot}$  for the case of aligned, non-synchronous rotation compared to the standard case. For the sake of convenience, we will write the standard Roche potential (1) and the potential for aligned, non-synchronous rotation (3) in dimensionless form (the distances are divided by  $A$ , the potential is divided by  $GM_1/A$ , and  $q = M_2/M_1$ ):

$$\Phi(\mathbf{r}) = -\frac{1}{\sqrt{x^2 + y^2 + z^2}} - \frac{q}{\sqrt{(x-1)^2 + y^2 + z^2}} - \frac{1}{2}(q+1) \left( (x-x_c)^2 + y^2 \right),$$

$$\Psi(\mathbf{r}) = -\frac{1}{\sqrt{x^2 + y^2 + z^2}} - \frac{q}{\sqrt{(x-1)^2 + y^2 + z^2}} - \frac{1}{2}(q+1) \left( (x-x_c)^2 + y^2 \right) - \frac{1}{2}(q+1)(f^2 - 1) (x^2 + y^2).$$

Figure 1 presents the dependencies of  $x_{L_1^{rot}}/x_{L_1}$  on  $q = M_2/M_1$  and  $f = \Omega_\star/\Omega$ . We can see that, when the rotation of the star is slower than the orbital rotation ( $f < 1$ ), the Roche lobe constructed with account for non-synchronous rotation is larger than the standard Roche lobe, with its maximum size achieved when  $f = 0$ . When the rotation of the star is faster than the orbital rotation, the "non-synchronous" Roche lobe is smaller than the standard Roche lobe, with  $x_{L_1^{rot}}/x_{L_1} \rightarrow 0$  for  $f \rightarrow \infty$ .

For the case of misaligned rotation, the expression for potential (2) becomes very complicated. We will specify the position of the vector  $\mathbf{\Omega}_\star$  by two angles: the angle  $\vartheta$  between  $\mathbf{\Omega}_\star$  and the  $Z$  axis, and the angle  $\phi$  between the  $X$  axis and the projection of  $\mathbf{\Omega}_\star$  onto the  $XY$  plane. The dimensionless potential can then be written

$$\begin{aligned} \Psi(x, y, z) = & -\frac{1}{\sqrt{x^2 + y^2 + z^2}} - \frac{q}{\sqrt{(x-1)^2 + y^2 + z^2}} \\ & + q(q+1)x - \frac{1}{2}(q+1)f^2\Delta^2(x, y, z) \end{aligned} \quad (4)$$

$$\begin{aligned} \Delta^2(x, y, z) = & x^2(1 - \cos^2 \phi \sin^2 \vartheta) + y^2(1 - \sin^2 \phi \sin^2 \vartheta) + z^2 \sin^2 \vartheta \\ & - xy \sin^2 \vartheta \sin 2\phi - xz \cos \phi \sin 2\vartheta - yz \sin \phi \sin 2\vartheta. \end{aligned}$$

In the case considered, the potential for the misaligned rotation depends on four parameters:  $q$ ,  $f$ ,  $\vartheta$ , and  $\phi$ . The last parameter changes with time, since the vector  $\mathbf{\Omega}_\star$  rotates with angular velocity  $-\Omega$  in a reference frame rotated with the binary system. The inner Lagrange point no longer lies on the line connecting the centers of the components. Moreover, according to [21], for some parameter values, the potential at the outer Lagrange point  $L_2$  can turn out to be lower than that at the inner Lagrange point. In this case, the Roche lobe will "open" from the side of  $L_2$  earlier, than it does from the side of  $L_1$ . However, as this occurs for large values of  $f$  and  $\vartheta$  (see Fig. 5 from [21]), we will not consider this possibility in our study.

Let us estimate how much the position of  $L_1$  deviates from the line connecting the component centers for the case of misaligned rotation. Given that, first,  $|y_{L_1^{rot}}| < |z_{L_1^{rot}}|$  for not very large  $\vartheta$ , and, second, the maximum of  $|z_{L_1^{rot}}|$  is reached when  $\phi = 0$ , we will estimate the deviation of  $L_1^{rot}$  from the line connecting the component centers using the value  $|z_{L_1^{rot}}|$  for  $\phi = 0$ . Our analysis of the vertical shift of the inner Lagrange point indicates that, for the adopted parameters, this deviation is negligible, since it is smaller than the cross section of the flow determined using standard models [34, 28].

This fact made it possible to simplify the model, and to assume that the shape of the star does not change as a function of orbital phase. The shape of the donor star is taken to be that of the equipotential surface (4) passing through  $L_1^{rot}$ . Since, for  $\phi = \pi/2$ , the inner Lagrange point  $L_1^{rot}$  lies along the line connecting the component centers, we used expression (4) for the potential with the fixed value  $\phi = \pi/2$  to determine the shape of the donor star.

### 1.3 Gasdynamical equations

The flow of gas in a binary system is described by a system of gas-dynamical equations:

$$\begin{aligned}
\frac{\partial \rho}{\partial t} + \frac{\partial \rho u}{\partial x} + \frac{\partial \rho v}{\partial y} + \frac{\partial \rho w}{\partial z} &= 0 \\
\frac{\partial \rho u}{\partial t} + \frac{\partial(\rho u^2 + P)}{\partial x} + \frac{\partial \rho uv}{\partial y} + \frac{\partial \rho uw}{\partial z} &= -\rho \frac{\partial \Phi}{\partial x} + 2\Omega v \rho \\
\frac{\partial \rho v}{\partial t} + \frac{\partial \rho uv}{\partial x} + \frac{\partial(\rho v^2 + P)}{\partial y} + \frac{\partial \rho vw}{\partial z} &= -\rho \frac{\partial \Phi}{\partial y} - 2\Omega u \rho \\
\frac{\partial \rho w}{\partial t} + \frac{\partial \rho uw}{\partial x} + \frac{\partial \rho vw}{\partial y} + \frac{\partial(\rho w^2 + P)}{\partial z} &= -\rho \frac{\partial \Phi}{\partial z} \\
\frac{\partial \rho E}{\partial t} + \frac{\partial \rho uh}{\partial x} + \frac{\partial \rho vh}{\partial y} + \frac{\partial \rho wh}{\partial z} &= -\rho u \frac{\partial \Phi}{\partial x} - \rho v \frac{\partial \Phi}{\partial y} - \rho w \frac{\partial \Phi}{\partial z}.
\end{aligned} \tag{5}$$

Here,  $\rho$  denotes density;  $u$ ,  $v$ , and  $w$  are the  $x$ ,  $y$ , and  $z$  components of the velocity vector  $\mathbf{v} = (u, v, w)$ ;  $P$  is the pressure;  $E = \varepsilon + 1/2 \cdot |\mathbf{v}|^2$  is the total specific energy;  $h = \varepsilon + P/\rho + 1/2 \cdot |\mathbf{v}|^2$  is the total specific enthalpy; and  $\Phi$  is the Roche potential. The gas-dynamical equations are written in a reference frame that rotates with the binary system, so that the Roche potential (1) is used in (5). To close the system of equations (5), we used the equation of state for an ideal gas,  $P = (\gamma - 1)\rho\varepsilon$ . To take into account radiative losses, we took the adiabatic index  $\gamma$  to be 1.01 [35, 36]. The non-synchronicity of the donor-star rotation was taken into account when specifying the boundary conditions.

## 1.4 Numerical model

To solve the above system of equations, we used the TVD scheme of Roe with a high approximation order [22, 37, 38]. The system of equations was solved from arbitrarily chosen initial conditions to the point when the flow regime became steady-state. The calculations for the case of aligned rotation included five orbital periods; the solution was stationary over the last three periods. In the case of misaligned rotation, it is impossible to achieve a true steady-state regime, due to the periodic time dependence of the boundary conditions. Therefore, we took the solution to be steady-state when the main features of the flow structure repeated with a period equal to that of the boundary conditions. We made calculations over six orbital periods, though strict periodicity of the solution was already seen for times longer than two orbital periods. The calculation area was the parallelepiped  $[-A...2A] \times [-A...A] \times [-A...A]$ . We used a nonuniform grid consisting of  $91 \times 81 \times 55$  nodes that were more densely spaced in the accretor zone.

We adopted free-outflow conditions for the matter at the accretor and at the outer boundary of the calculation zone. We used (4) to determine the shape of the donor star, which coincided with the equipotential surface passing through the inner Lagrange point  $L_1^{rot}$  for  $\phi = \pi/2$ . The boundary conditions at the surface of this star were determined by solving for the decay of the discontinuity between the gas parameters  $(\rho_0, \mathbf{v}_0, P_0)$  at the surface of the mass-losing star and in the calculation cell that was nearest to the given point of the surface [35]. Note that the boundary value of the density does not affect the solution, since the system of equations scales in  $\rho$  and  $P$ . In the calculations, we chose an arbitrary value of  $\rho_0$ ; to determine the real densities in a specific system with a known mass-loss rate, the calculated densities must simply be increased in accordance with a scale determined from the ratio of the real and model densities at the surface of the mass-losing component.

The velocity at the surface of the donor star was specified as

$$\mathbf{v}_0 = \boldsymbol{\Omega}_*^{rot} \times \mathbf{r} + \mathbf{n}c_0,$$

where  $\boldsymbol{\Omega}_*^{rot} = \boldsymbol{\Omega}_* - \boldsymbol{\Omega}$  is the angular-velocity vector for the rotation of the donor star in the rotating reference frame,  $c_0$  is the sound speed at the stellar surface, and  $\mathbf{n}$  is the normal vector to the stellar surface. Note that our assumption that the star's rotation is uniform implies that the velocity vector at the surface of the donor star has a component normal to the surface, which is due, not only to the sound speed, but also to the rotation of the star. It is evident that, in the equilibrium state for the stellar surface, no non-thermal movement of gas can occur normal to the surface.

Under the assumption of uniform rotation, the star should have the shape of an spheroid that extends to  $L_1^{rot}$ . However, the shape calculated using the total potential does not yield such a solution, since an additional velocity component



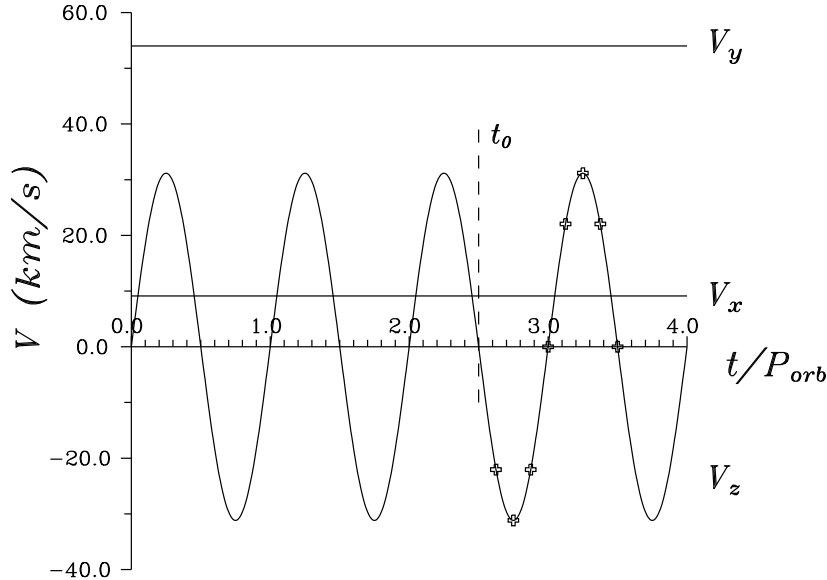


Figure 2: Components of velocity vector at the inner Lagrange point for various cases: (1) synchronous rotation  $V_x = c_0$ ,  $V_y = 0$ ,  $V_z = 0$ ; (2) aligned, non-synchronous rotation  $V_x = c_0$ ,  $V_y = x_{L_1^{rot}} \Omega_\star^{rot}$ ,  $V_z = 0$ ; (3) misaligned, non-synchronous rotation for  $\vartheta^* = 30^\circ$  (the angle between the rotation vector in the rotating reference frame  $\Omega_\star^{rot}$  and the  $Z$  axis):  $V_x = c_0$ ,  $V_y = x_{L_1^{rot}} \Omega_\star^{rot} \cos(\vartheta^*)$ ,  $V_z = -x_{L_1^{rot}} \Omega_\star^{rot} \sin(\vartheta^*) \sin(-\Omega t)$ . The markers correspond to eight times  $t = t_0 + 1/8 P_{orb}$ ,  $t = t_0 + 1/4 P_{orb}$ ,  $t = t_0 + 3/8 P_{orb}$ ,  $\dots$ ,  $t = t_0 + P_{orb}$ , for which the distributions of gas-dynamical parameters are presented further in Figs. 4c, 7c, and 9.

normal to the surface arises due to the non-spherical shape of the star. This implies that the adopted law for the rotation of the star is not self-consistent. The problem of determining a self-consistent rotation law for a star in a binary system remains unsolved, with the exception of two special cases: synchronous rotation and the case when the angular-momentum vector of the donor star is zero in the laboratory frame. Simultaneously using in the gas-dynamical model the shape of the stellar surface obtained and the gas-velocity boundary conditions determined assuming uniform rotation, we obtain a partially self-consistent solution for this problem. In the model considered, the gas outflowing from the surface of the donor star under the adopted boundary conditions can form new outer layers of the donor star, thereby adjusting the self-consistent solution. Unfortunately, the presence of additional forces (the Coriolis force and pressure gradient, which are not included in the potential) means that we can only approximate a self-consistent solution; however, this approach seems optimal for this stage of our study.

## 2 CALCULATION RESULTS

To analyze the impact of the rotation of the donor star on the structure of mass flows in the system, we compared models with synchronous rotation (previous results, presented in [22-25]), with non-synchronous, aligned rotation, and with non-synchronous, misaligned rotation of the mass-losing star. We specified the boundary value of the gas velocity at the surface of the donor star using (6); for both models with non-synchronous rotation, the rotational velocity of the star in the laboratory frame was assumed to be twice the angular rotation velocity of the system. For the calculation with misaligned rotation, the stellar rotation vector was taken to be inclined to the  $Z$  axis by  $15^\circ$  in the laboratory frame (the inclination angle in the rotating frame was  $\vartheta^* = 30^\circ$ ).

The different model calculations differ only in the adopted boundary values for the velocity at the surface of the donor star. Figure 2 presents the components of the velocity vector at the inner Lagrange point for all cases. In the adopted reference frame, the case of synchronous rotation corresponds to the existence of only the velocity component  $V_x$ , while  $V_y = V_z = 0$ . In the case of aligned, non-synchronous rotation, only  $V_z = 0$ , and in the case of misaligned, non-synchronous rotation all velocity components are non-zero, with  $V_z$  being a periodic function of time. The differences in the boundary conditions at the surface of the mass-losing star lead, in particular, to changes in the parameters for the matter flowing through the vicinity of the inner Lagrange point, as shown in Fig. 3. Figures 3a and 3b show surfaces of constant density in the vicinity of the inner Lagrange point at the level  $\rho = 0.02\rho_{L_1}$  for the cases of synchronous and aligned non-synchronous rotation. The cross section of the  $YZ$  plane that forms the edge of the plot in Fig. 3 is close to  $L_1$  (at a distance of  $0.066A$ ). The projection of the inner Lagrange point onto the  $YZ$  cross section is marked by a dot. For the case of misaligned, non-synchronous rotation, the adopted boundary conditions, and consequently the solution obtained, are time dependent. Figures 3c and 3d present surfaces of constant density near the inner Lagrange point at the level  $\rho = 0.02\rho_{L_1^{rot}}$  for the two times  $t = t_0 + \frac{3}{8}P_{orb}$  and  $t = t_0 + \frac{3}{4}P_{orb}$ , illustrating the change of the flow parameters, and especially the shift of the flow relative to the orbital plane. Comparison of Figs. 3a–d shows that the flow parameters differ substantially for the different cases, which, in turn, should lead to changes of the flow patterns obtained for the different types of donor-star rotation.

The solutions obtained for synchronous [22–25] and aligned, non-synchronous rotation are steady-state. The basic properties of the obtained flow patterns are shown in Figs. 4a and 4b, which show surfaces of constant density at the level  $\rho = 0.004\rho_{L_1}$  for both model calculations. For the case of misaligned, non-synchronous rotation, we considered the solution to be steady-state when the main features of the flow structure repeated with the period of the boundary conditions. Figure 4c presents surfaces of constant density at the level  $\rho = 0.004\rho_{L_1^{rot}}$  for eight times (Fig. 2) covering the total variation period for the boundary conditions. Analysis

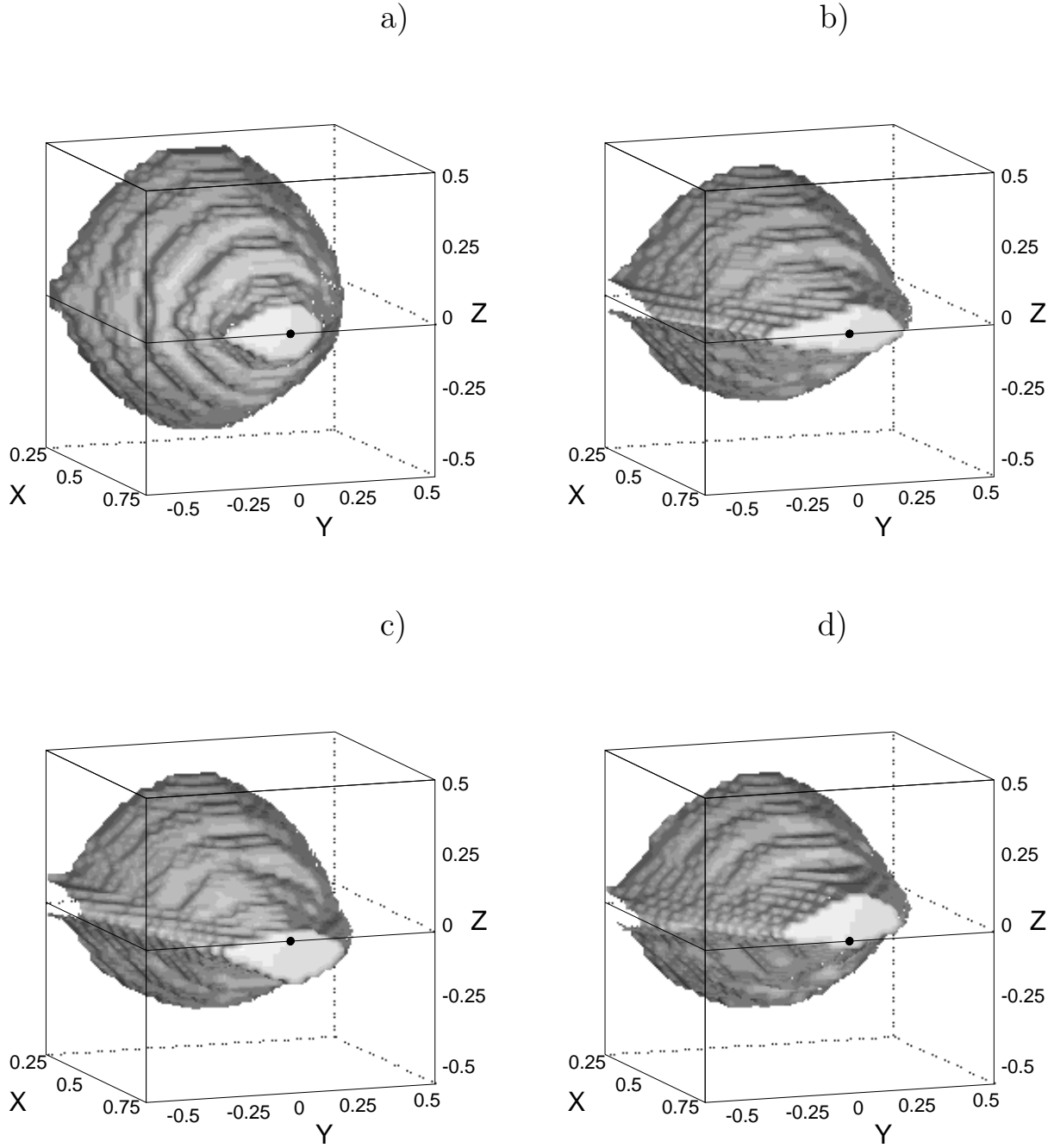


Figure 3: Surface of constant density in the vicinity of the inner Lagrange point at the level  $\rho = 0.02\rho_{L_1}$  for the cases of: (a) synchronous rotation; (b) non-synchronous, aligned rotation; (c) and (d) non-synchronous, misaligned rotation for times  $t = t_0 + \frac{3}{8}P_{orb}$  and  $t = t_0 + \frac{3}{4}P_{orb}$ , respectively. The cross section in the  $YZ$  plane was made at a distance of  $0.066A$  from  $L_1$ . The thick dot marks the projection of the inner Lagrange point onto the  $YZ$  cross section.

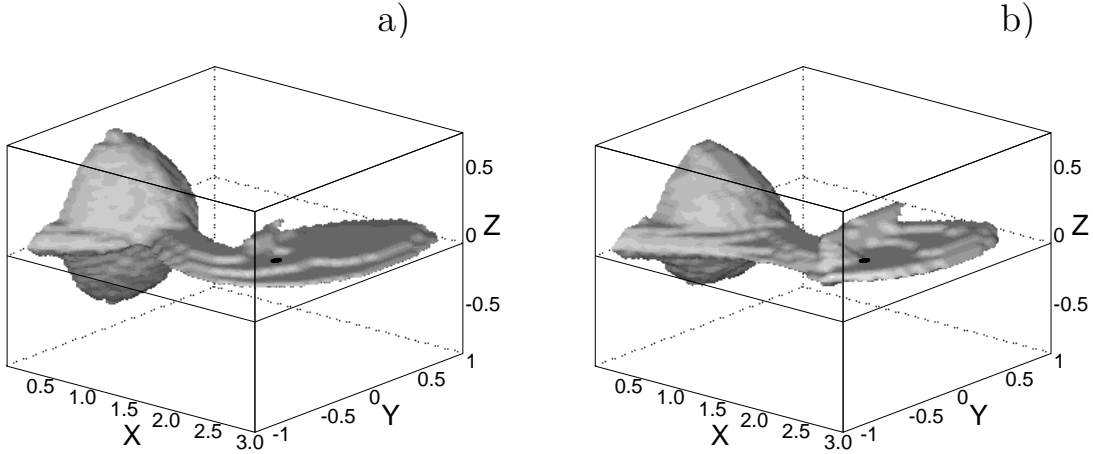


Figure 4: *Surface of constant density at the level  $\rho = 0.004\rho_{L_1}$  for the case of (1) synchronous rotation and (b) non-synchronous, aligned rotation. The thick dot marks the position of the accretor.*

of the results presented in Fig. 4c shows that the behavior of the matter in and around the disk reflects changes in the injected matter (as well as changes in the boundary conditions at the surface of the donor star). This implies that a driven-disk model has been realized in our calculations. An additional illustration of this fact is provided by Fig. 5, which shows the temporal dependencies of variations in the  $Z$ -coordinates of the center of mass of the accretion disk and of the velocity at the inner Lagrange point. Analysis of the curves presented in Fig. 5 confirms the "driven" character of the solution, and the strict dependence of the flow pattern near the accretor on the behavior of the flow in the vicinity of  $L_1$ . Note that the inclination angle of the normal to the disk surface to the  $Z$  axis is  $\pm 10^\circ$  in the  $XZ$  plane and  $\pm 20^\circ$  in the  $YZ$  plane.

Let us consider the details of the flow pattern obtained. For the cases of synchronous and aligned, non-synchronous rotation, the main features of the steady-state flow pattern obtained are clearly visible in Figs. 4a,b and 6a,b. Our results indicate that the rarefied gas of the circumbinary envelope (stream lines 'a' and 'b') has an appreciable impact on the structure of gas flows in the system. The gas of the circumbinary envelope interacts with the matter flowing from the vicinity of  $L_1$  and deflects it, leading to a shock-free (tangential) interaction of the flow with the outer edge of the forming accretion disk (stream line 'c'), and, consequently, to the absence of a "hot spot" on the disk. At the same time, the interaction of the circumbinary-envelope gas (stream line 'b') with the flow leads to the formation of an extended shock of variable intensity along the edge of the flow. The impact of aligned, non-synchronous rotation of the donor star is manifested only in a number of quantitative changes, while the overall flow pattern remains qualitatively similar.

As noted above, in the case of non-synchronous rotation, the existence of a

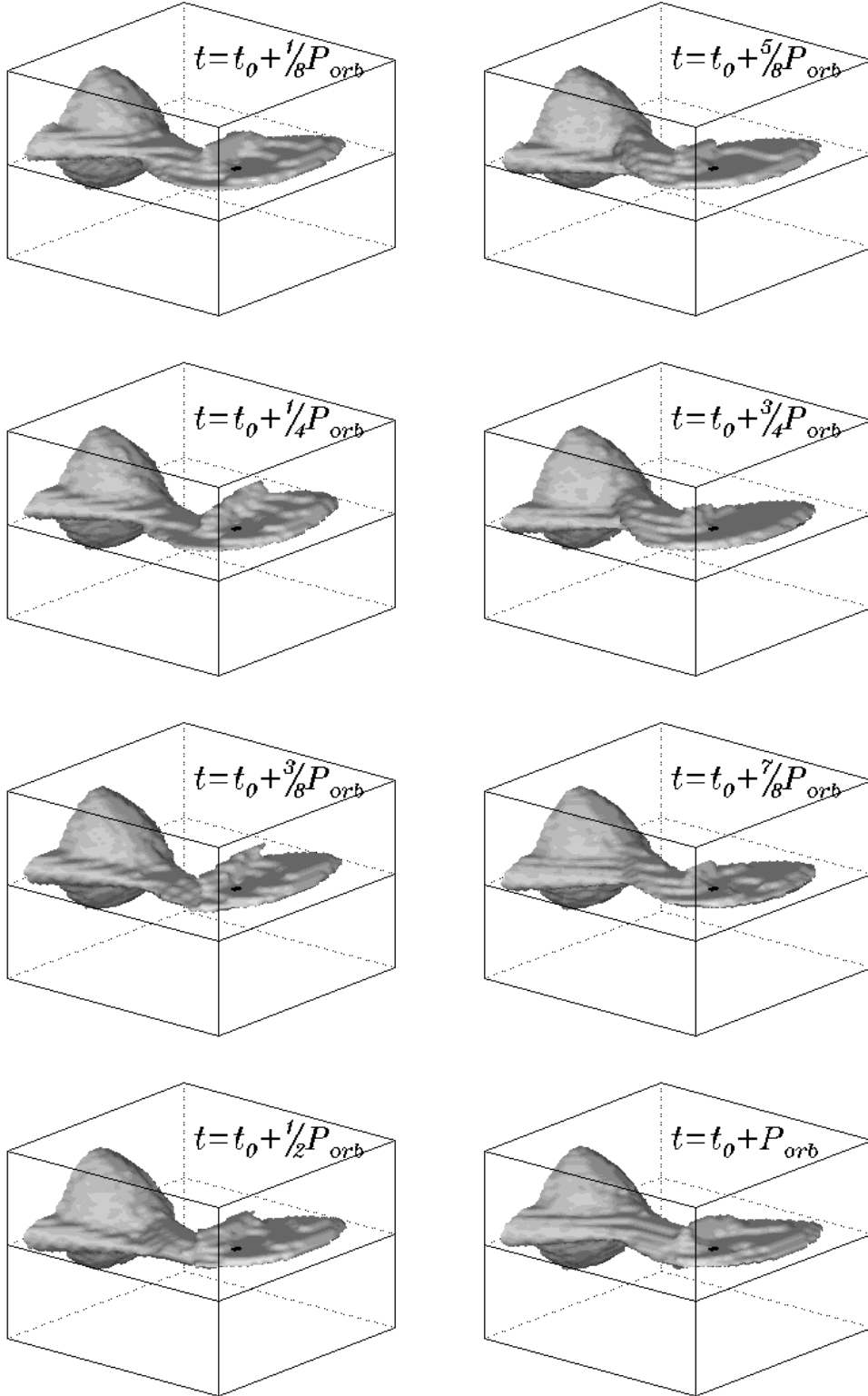


Figure 4c: Surface of constant density at the level  $\rho = 0.004\rho_{L^{\text{rot}}}$  for the case of non-synchronous misaligned rotation for the eight times indicated in Fig. 2. The size of the area displayed for (c) are the same as for (a) and (b). The thick dot marks the position of the accretor.

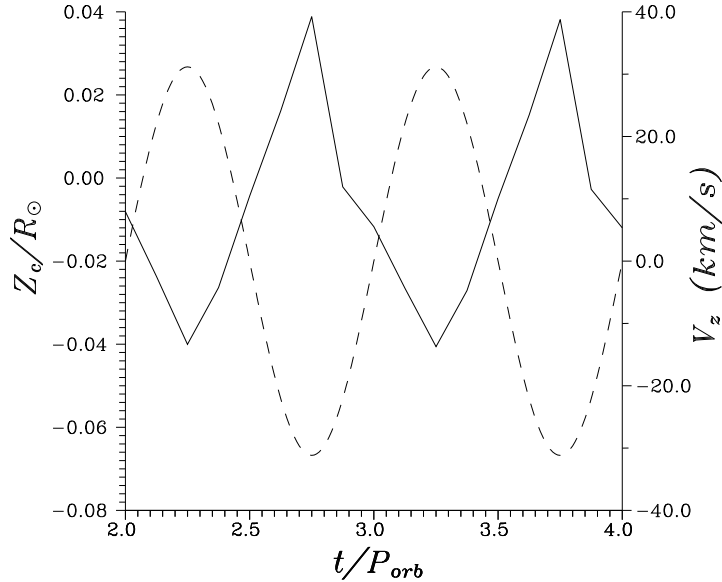
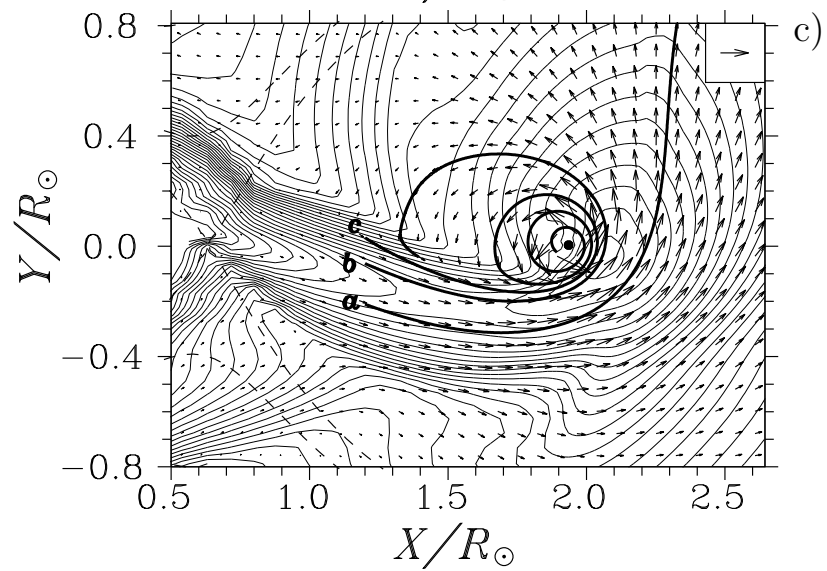
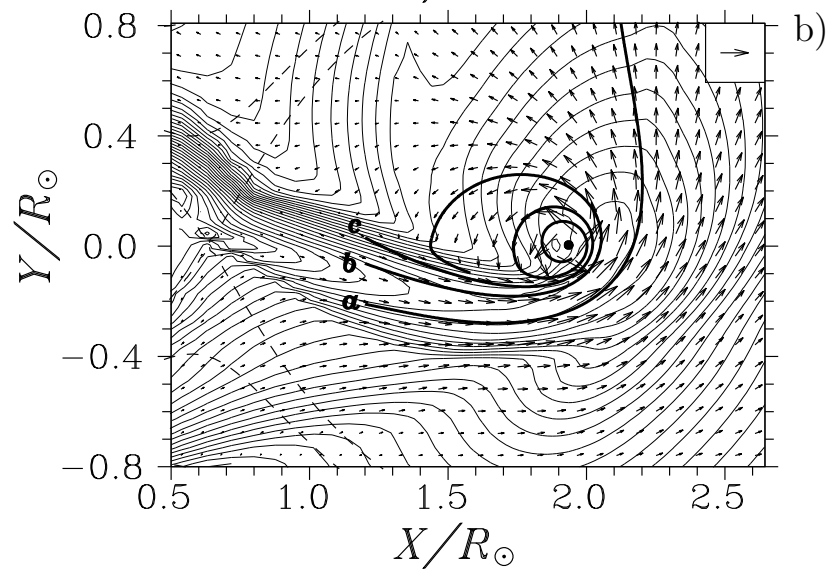
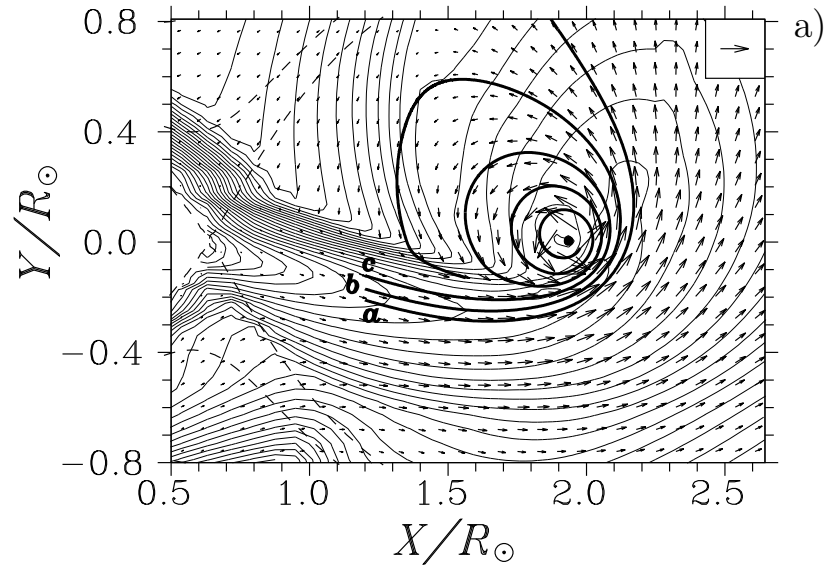


Figure 5:  $Z$  coordinate of the center of mass of the accretion disk for the case of non-synchronous, misaligned rotation as a function of time. The dashed line marks the  $Z$  component of the velocity at the inner Lagrange point.

$V_y$  component for the velocity brings about changes in the parameters of the inflowing matter (Fig. 3). Because of the shift of the flow near  $L_1$ , the flow approaches the accretor as it advances, and the disk that forms is substantially smaller than in the case of synchronous rotation (Figs. 6a,b). In our calculation for non-synchronous rotation, the thicknesses of the flow, the accretion disk, and the structures surrounding the disk exceed the disk thickness in the synchronous case (Figs. 7a,b; 8a,b). Note that, in addition to forming a shock, the interaction of the rarefied gas of the circumbinary envelope (stream line ‘b’ in Fig. 6) with the flow also leads to the formation of gaseous ”clouds” that precede the front edge of the flow outside the disk-formation area (Figs. 4, 8). The appearance of these formations is associated with the interaction (collision) of rarefied envelope gas outside the equatorial plane with the flow. The larger thickness of the flow in the case of aligned, non-synchronous rotation brings about the formation of

Figure 6: (Next page) Lines of constant density and velocity vectors in the equatorial ( $XY$ ) plane for the case of (a) synchronous rotation; (b) non-synchronous, aligned rotation; and (c) non-synchronous, misaligned rotation for time  $t = t_0 + \frac{3}{8}P$ . The thick dot marks the position of the accretor. The dashed curves depict the Roche equipotentials. The vector in the top right corner corresponds to a velocity of 800 km/s. Stream lines for the flowing matter are denoted ‘a’, ‘b’, ‘c’.



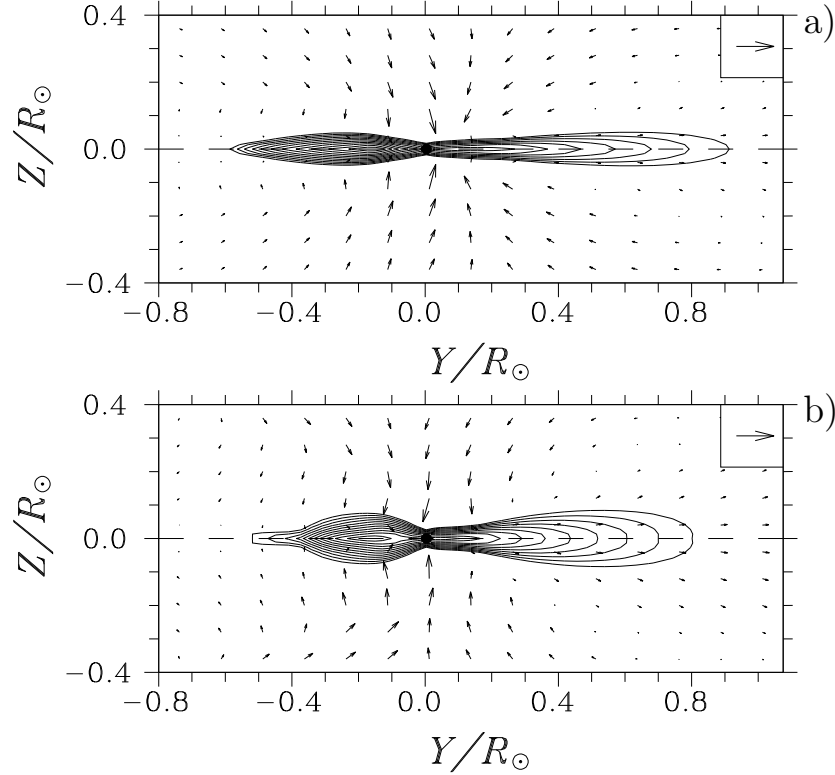


Figure 7: Lines of constant density and velocity vectors in the plane perpendicular to the line connecting the centers of the stars (the  $YZ$  plane) passing through the accretor for the case of (a) synchronous rotation, and (b) non-synchronous, aligned rotation. The last isoline corresponds to a density of  $\rho = 0.005\rho_{L_1}$ . The thick dot marks the position of the accretor. The vector in the top right corner corresponds to a velocity of 1500 km/s.

more pronounced "clouds".

In the calculations for misaligned, non-synchronous rotation, all the basic features of the flow inherent to our previous calculations are maintained. Characteristic properties, such as the formation of a circumbinary envelope, the absence of a "hot spot" at the edge of the accretion disk, and the formation of a shock wave along the edge of the flow, are clearly visible in Figs. 4c and 6c. As noted above, a "driven disk" is realized in this case, and there are periodic changes in the solution in the steady-state regime (Figs. 4c, 5, 7c). Unlike the case of aligned, non-synchronous rotation, the matter in the disk and the surrounding structures fluctuate about the equatorial plane, leading to the formation of complicated flow structures ("tracks"). The presence of these "tracks" of matter means that the disk that forms possesses intermediate linear size and thickness, between those for the models with synchronous and aligned, non-synchronous rotation (Figs. 6, 7, 8). Due to the "driven" character of the solution, the formation of "clouds"



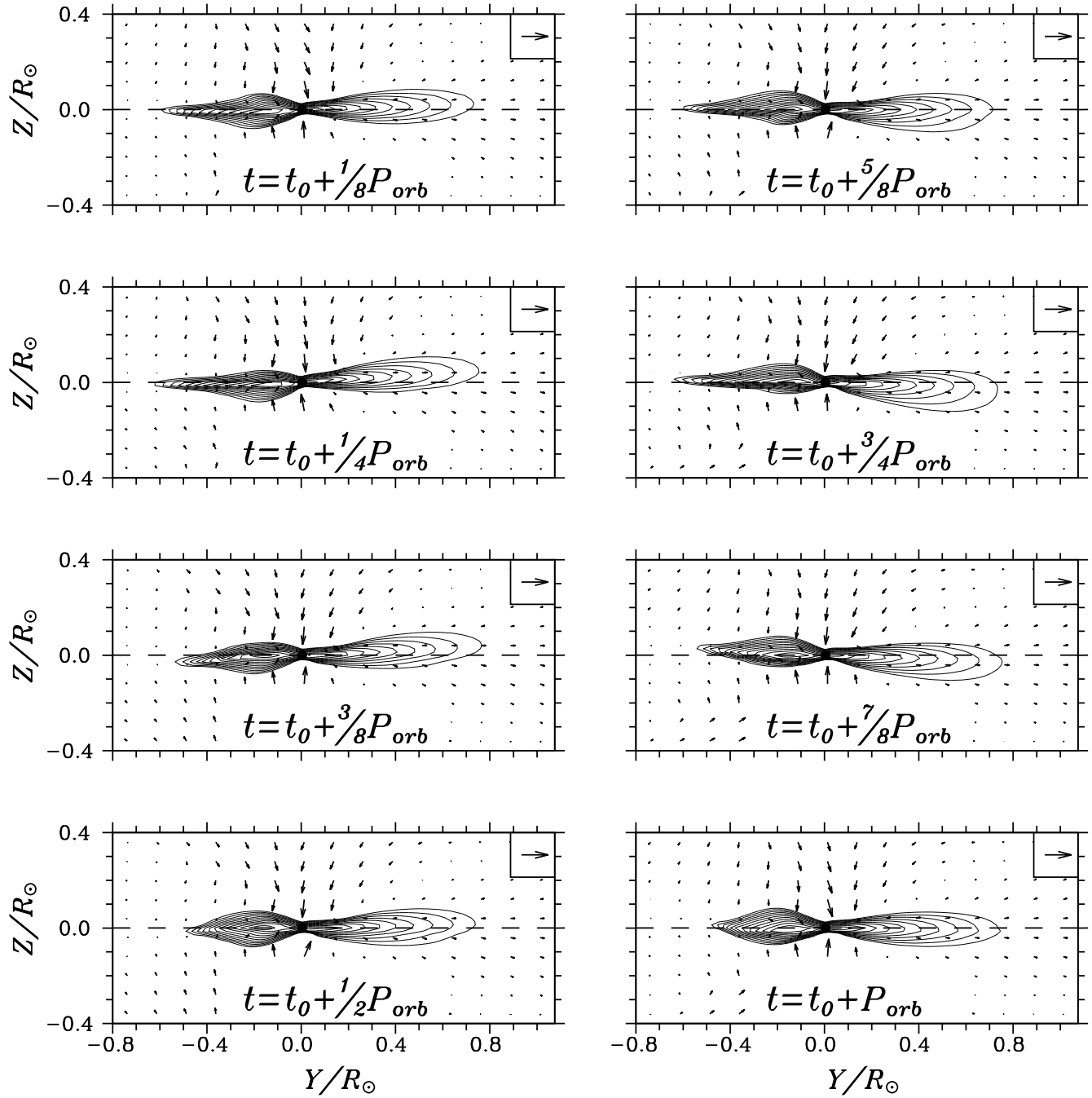


Figure 7c: Lines of constant density and velocity vectors in the plane perpendicular to the line connecting the centers of the stars (the  $YZ$  plane) passing through the accretor for the case of non-synchronous, misaligned rotation for the eight times indicated in Fig. 2. The last isoline corresponds to a density of  $\rho = 0.005\rho_{L_1^{rot}}$ . The thick dot marks the position of the accretor. The vector in the top right corner corresponds to a velocity of 1500 km/s.

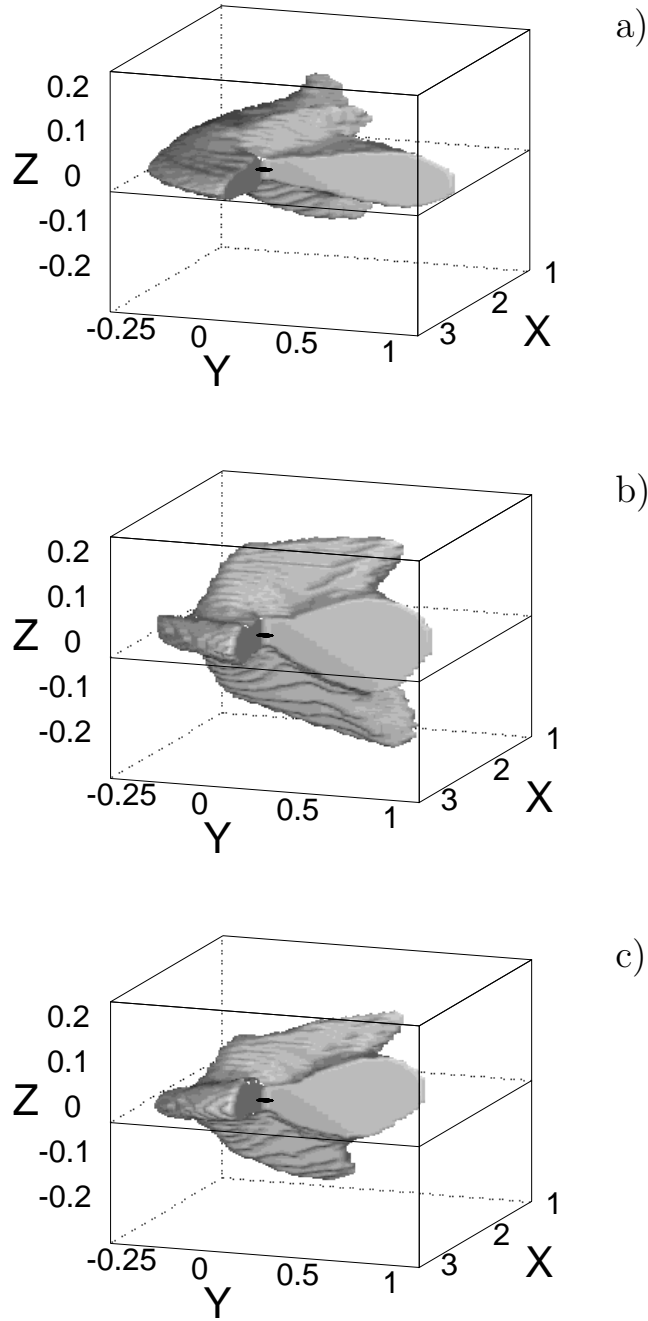


Figure 8: Surface of constant density near the accretor at the level  $\rho = 0.004\rho_{L1}$  for the case of (a) synchronous rotation; (b) non-synchronous, aligned rotation; and (c) non-synchronous, misaligned rotation for time  $t = t_0 + \frac{3}{8}P$ . The thick dot marks the position of the accretor. The cross section of the surface made by the half-planes  $y = 0$  ( $x > A$ ) and  $x = A$  ( $y > 0$ ) also shown.

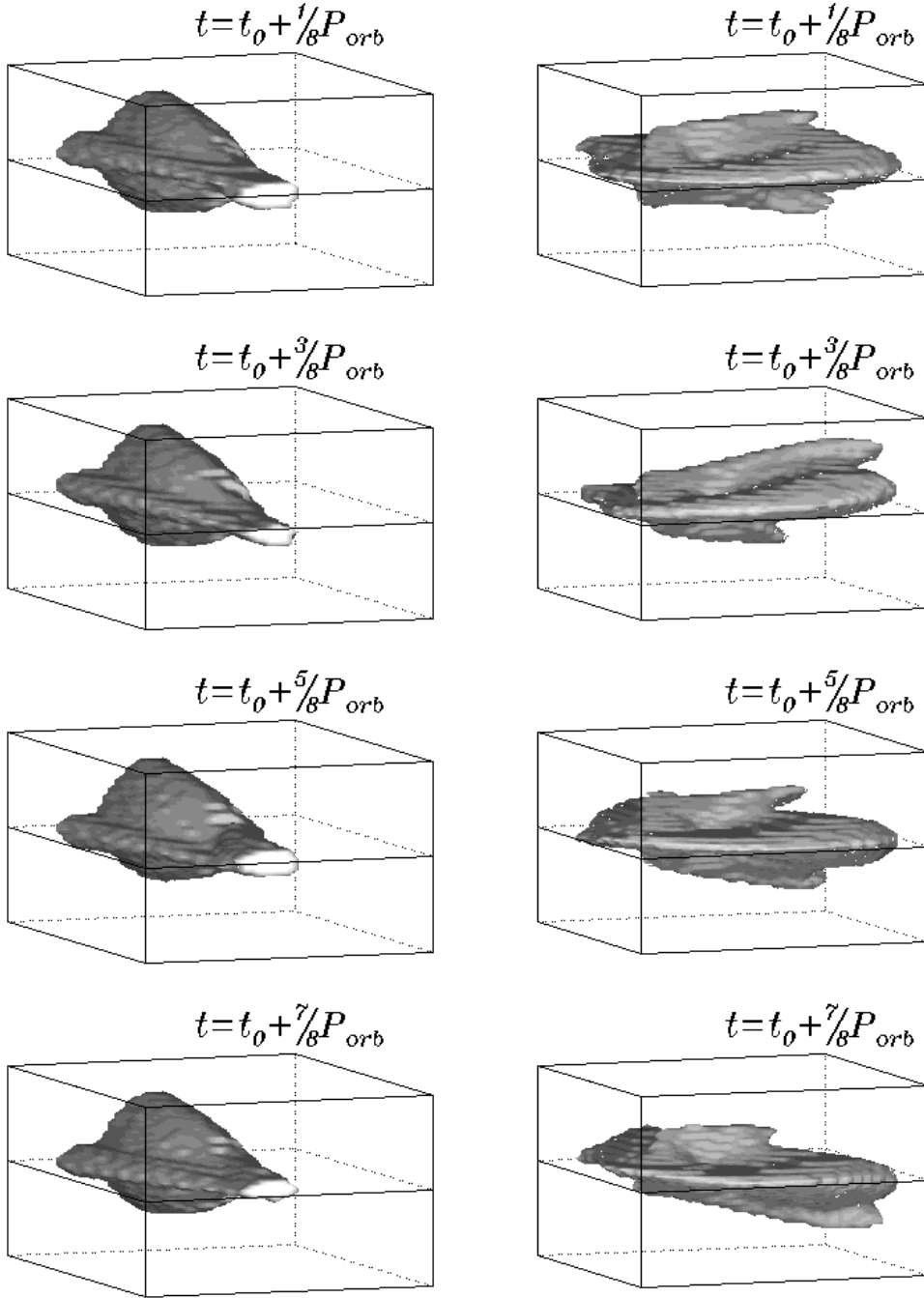


Figure 9: Surfaces of constant density at the level  $\rho = 0.0025\rho_{L_1^{rot}}$  for the case of non-synchronous, misaligned rotation at four times in the vicinity of the inner Lagrange point (left) and the accretion disk (right). The sizes of the depicted areas are  $[0..5R_\odot] \times [-4R_\odot..4R_\odot] \times [-3R_\odot..3R_\odot]$  (left) and  $[4R_\odot..11R_\odot] \times [-3R_\odot..4R_\odot] \times [-2R_\odot..2R_\odot]$  (right).

(gaseous formations above and below the equatorial plane) is also periodic (Fig. 9). Since it is not excluded that these formations can contribute to the total emission of the system, together with the emission of the disk and surrounding material, the periodicity of their formation should be considered when interpreting observations.

## CONCLUSIONS

We have presented the results of three-dimensional numerical modeling of the mass transfer in semi-detached binary systems with rotation of the mass-losing star. We considered the cases of both aligned and misaligned, non-synchronous rotation of the donor star, and compared the flow patterns obtained with the synchronous case.

Our analysis indicates that the main features of the flow are qualitatively similar for all the calculations. Study of the flow structure indicates that the rarefied gas of the circumbinary envelope has an appreciable impact on the structure of gas flows in the system. The circumbinary-envelope gas interacts with the matter flowing from the vicinity of  $L_1$  and deflects it, leading to a shock-free (tangential) interaction of the flow with the outer edge of the forming accretion disk, and, consequently, to the absence of a "hot spot" on the disk. At the same time, the interaction of this gas with the flow forms an extended shock of variable intensity along the edge of the flow.

Unlike the cases of synchronous and aligned, non-synchronous rotation of the donor star, in the case of misaligned, non-synchronous rotation, it is impossible to achieve a genuine steady-state regime due to the periodic time dependence of the boundary conditions. Therefore, in the misaligned, non-synchronous case, the solution was considered to be steady-state when the basic features of the flow structure repeated with the period of the boundary conditions. Our analysis indicates that the behavior of the disk and surrounding material reflects changes in the injected matter (or changes in the boundary conditions at the surface of the donor star). This implies that a "driven disk" model has been realized in our calculations. The inclination angle of the normal vector to the disk surface to the  $Z$  axis is  $\pm 10^\circ$  in  $XZ$  plane and  $\pm 20^\circ$  in the  $YZ$  plane. The calculated periodic changes of the shape of the accretion disk and of the surrounding gaseous envelope should be observable via the associated changes in the emission of this region.

## ACKNOWLEDGMENTS

This work was supported by the Russian Foundation for Basic Research (project code 96-02-16140) and the INTAS Foundation (grant 93-93-EXT).

## REFERENCES

1. Tassoul, J.-L. 1978 *Theory of rotating stars*, Princeton Univ. Press, Princeton
2. Wilson, R.E., Van Hamme, W., & Petera, L.E. 1985, ApJ, 289, 748
3. Van Hamme, W., & Wilson, R.E. 1992, AJ, 92, 1168
4. Habets, G.M.H.J., & Zwaan, C. 1989, A&A, 211, 56
5. Griffin, R., & Griffin, R. J. 1986, A&A, 7, 45
6. Fekel, F.C., Moffet, T.J., & Henry, G.W. 1986, ApJS, 60, 551
7. Shcherbakov, A.G., Tuyominen, I., Jetsu, L., Katsova M.M., & Poutanen M. 1990, A&A, 235, 205
8. Ayres, T.R. 1991, ApJ, 375, 704
9. Katsova, M.M. 1990, Lect. Notes Phys., 397, 220
10. Shakura, N.I. 1972, Astron. Zh., 49, 921 (Sov. Astron., 16, 756)
11. Roberts, W.J. 1974, ApJ, 187, 575
12. Petterson, J.A. 1975, ApJ, 201, L61
13. Katz, J.I. 1979, ApJ, 236, L127
14. Shklovskii, I.S. 1979, Pis'ma Astron. Zh., 5, 644 (Sov. Astron. Lett., 5, 344)
15. Van den Heuvel, E.P.J., Ostriker, J.P., & Petterson, J.A. 1980, A&A, 81, 27
16. Whitmire, D.P., & Matese, J.J. 1980, MNRAS, 193, 707
17. Cherepashchuk, A.M. 1981, Pis'ma Astron. Zh., 7, 201 (Sov. Astron. Lett., 7, 111)
18. Kruszewski, A. 1964, Acta Astron., 14, 231
19. Belvedere, G., Lanzafame, G., & Molteni, D., 1993, A&A, 280, 525
20. Lanzafame, G., Belvedere, G., & Molteni, D. 1994, MNRAS, 267, 312
21. Avni, Y., & Schiller, N. 1982, ApJ, 257, 703

22. Bisikalo, D.V., Boyarchuk, A.A., Kuznetsov, O.A., & Chechetkin, V.M. 1997, *Astron. Zh.*, 74, 880 (*Astron. Reports*, 41, 786; preprint astro-ph/9802004)
23. Bisikalo, D.V., Boyarchuk, A.A., Kuznetsov, O.A., & Chechetkin, V.M. 1997, *Astron. Zh.*, 74, 889 (*Astron. Reports*, 41, 794; preprint astro-ph/9802039)
24. Bisikalo, D.V., Boyarchuk, A.A., Chechetkin, V.M., Molteni D., & Kuznetsov O.A. 1998, *MNRAS*, 300, 39 (preprint astro-ph/9805261)
25. Bisikalo, D.V., Boyarchuk, A.A., Kuznetsov, O.A., & Chechetkin, V.M. 1998, *Astron. Zh.*, 75, 706 (*Astron. Reports*, 42, 706; preprint astro-ph/9806013)
26. Armitage, P.J., & Livio, M. 1996, *ApJ*, 470, 1024
27. Kopal, Z. 1978, *Dynamics of close binary systems*, Reidel, Dordrecht
28. Pringle, J.E., & Wade, R.A. (Eds.) 1985, *Interacting binary stars* Cambridge Univ. Press, Cambridge
29. Plavec, M. 1958, *Mém. Soc. Roy. Sci. Liège*, 20, 411
30. Kruszewski, A. 1963, *Acta Astron.*, 13, 106
31. Limber, D.N. 1963, *ApJ*, 138, 1112
32. Kruszewski, A. 1966, *Adv. Astron. Astrophys.*, 4, 233
33. Layton, J.T., Blondin, J.M., Owen, M.P., & Stevens, I.R. 1998, *New Astron.*, 3, 111
34. Lubow, S.H., & Shu, F.H. 1975, *ApJ*, 198, 383
35. Sawada, K., Matsuda, T., & Hachisu, I. 1986, *MNRAS*, 219, 75
36. Bisikalo, D.V., Boyarchuk, A.A., Kuznetsov, O.A., Chechetkin V.M. 1995, *Astron. Zh.*, 72, 367 (*Astron. Reports*, 39, 325)
37. Roe, P.L. 1986, *Ann. Rev. Fluid. Mech.*, 18, 337
38. Osher, S., & Chakravarthy, S. 1984, *SIAM J. Numer. Anal.*, 21, 955